Catena 198 (2021) 105027

Contents lists available at ScienceDirect

Catena

journal homepage: www.elsevier.com/locate/catena

A carbon-sink in a sacred forest: Biologically-driven calcite formation in highly weathered soils in Northern Togo (West Africa)

Hafeez Ur Rehman [a,*], Rosa M. Poch [b], Fabio Scarciglia [c], Michele L. Francis [d]

[a] Faculty of Science and Technology, Norwegian University of Life Sciences, Ås, Norway
[b] Departament de Medi Ambient i Ciències del Sòl, Universitat de Lleida, Catalonia, Spain
[c] Dipartimento di Biologia, Ecologia e Scienze della Terra, Università della Calabria, Italy
[d] Department of Soil Science, University of Stellenbosch, South Africa

ARTICLE INFO

Keywords:
Pedodiversity
Organic matter
Granite and gneiss
Calcium oxalate
Weathering
Palygorskite

ABSTRACT

Soil organic matter (OM) is a source of fertility for food provisioning and a means for climate mitigation. A high pedodiversity observed over very short distances due to both past and present land use, such as in Western Africa (Northern Togo), makes this a crucial issue. In particular, some small spots covered by sacred forests (*forêts sacrées*) of high cultural value in this area are extremely biodiverse, calcareous and high in OM in contrast with the non-calcareous, poor OM, overgrazed woody savannah and agricultural surroundings. The objectives of our work were to understand this pedodiversity and the process of $CaCO_3$ formation in the soil under the highly biodiverse forest using morphological, micromorphological, chemical and mineralogical soil analyses. The results show a high degree of weathering of the gneiss parent material, presence of plinthite gravels, dominance of 1:1 clays, formation of swelling clays in the imperfectly drained soils, and low OM content. The presence of palygorskite, although in traces, suggests drier intervals and is consistent in this context with the extreme wet and dry climate conditions in the region. In the OM rich soils under forest, bio-calcification takes place in the form of $CaCO_3$ needles, micrite hypocoatings around biopores and calcified cells. Oribatid excrements are associated with calcite and organic matter in the sacred forest soil, indicating that litter recycling has played an important role in the formation of calcite. We hypothesize that the high biological activity releasing CO_2, formation of HCO_3^- and precipitation of $CaCO_3$ due to the Ca^{2+} released by the recycled organic matter and weathering of plagioclases, lead to different forms of secondary calcium carbonate in the sacred forest soils. The high oxalate content of the vegetation in the sacred forest suggests that calcium carbonate formation, possibly via the oxalate-carbonate pathway, may also have played a role in calcite precipitation in these in organic matter rich soils. The parent material of these soils is not calcareous, meaning that these are not lithogenic carbonates, thus making them an important carbon sink. The soil characteristics indicate a high potential for development of the soils of the area in both agricultural yields and in potential carbon sequestration relevant to global change policies.

1. Introduction

Across Benin and Togo (Dahomey Gap, West Africa, Fig. 1), sacred forests (*forêts sacrées*) represent islands of pedo- and biodiversity in the middle of overgrazed woody semiarid savannahs and croplands (Kokou and Sokpon, 2006; Poch and Ubalde, 2006). A "sacred forest" is a forest that is used for religious purposes and is believed to be inhabited and protected by gods, totem animals or ancestors. These forests cover several hundred square kilometers, and some researchers claim that they are the remnants of a once continuous forest along the West African coast (Fairhead and Leach, 1998). The cultural or religious significance of sacred forests in West Africa has contributed significantly to the conservation of these forest resources (Bhaghwat et al., 2005; Ceperley et al., 2010; Fraser et al., 2016; Irakiza et al., 2016; Kibet, 2011; Kokou and Dzifa, 2007; Upadhaya et al., 2003). Due to their tendency to be maintained over long periods of time, sacred forests often contain ecological communities that have otherwise been removed from a region (Fig. 2) and these forests remnants consequently play an important role in the conservation of biodiversity (Campbell, 2004; Sanou et al., 2013).

* Corresponding author.
E-mail addresses: hafeez.ur.rehman@nmbu.no, hafeezrehman2011@hotmail.com (H. Ur Rehman).

https://doi.org/10.1016/j.catena.2020.105027
Received 9 May 2020; Received in revised form 17 October 2020; Accepted 1 November 2020
Available online 10 November 2020

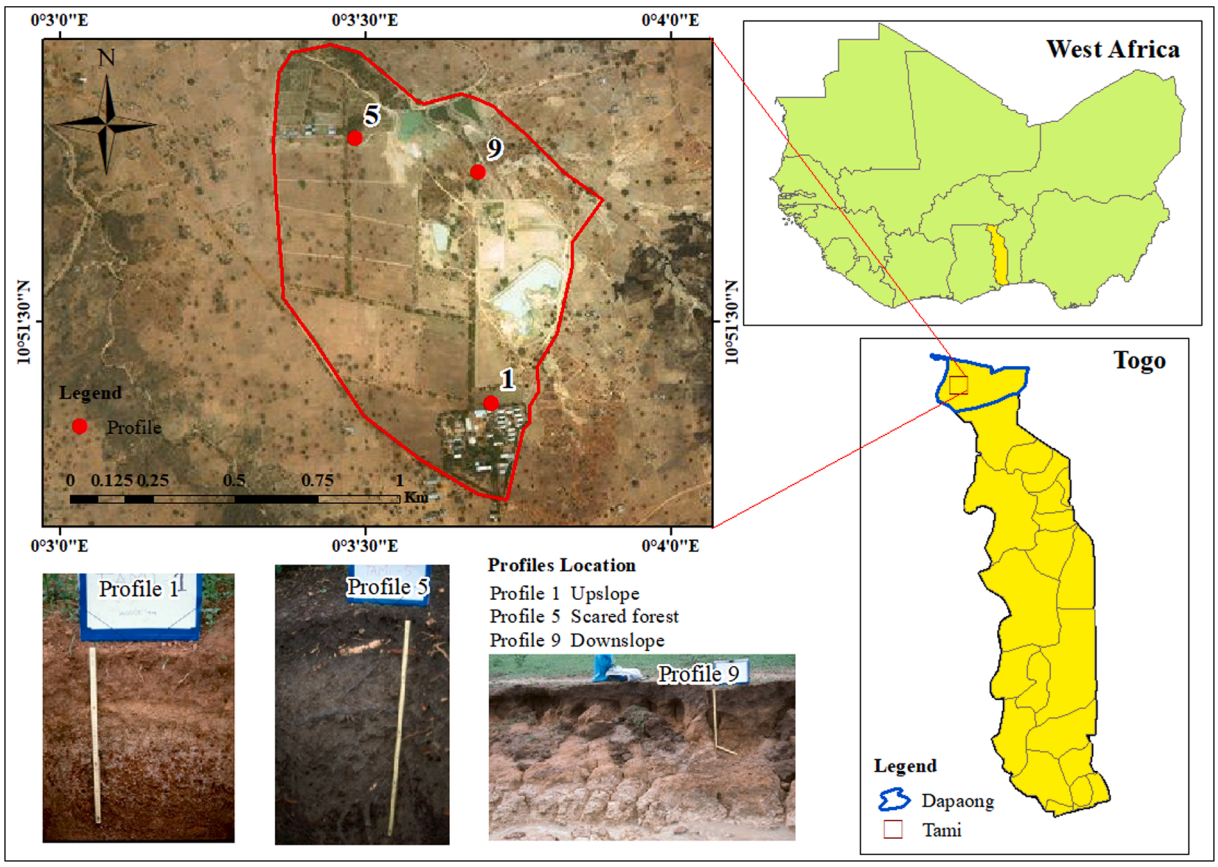

Fig. 1. Map of West Africa indicating Tami area in Togo, with profiles 1, 5 and 9, and the location of the study site (Tami).

Local communities establish rules that vary between regions, including prohibition of reckless timber and game harvesting, thus tempering natural resource exploitation and persevering the scared forests and their biodiversity over many generations (Ceperley et al., 2010). According to Daye and Healey (2015) and Kokou et al. (2008), local communities have a greater respect for sacred forests than they have for government-protected areas which are vulnerable and are being affected by degradation. Nonetheless, the sacred forests are becoming rarer and more fragmented as they are increasingly threatened by population growth, expansion of buildings, construction of roads, and erosion of traditional religious beliefs. The importance of a sustainable forest management to maintain ecosystem functions and preserve biological diversity has grown since 1992, after the United Nations Conference on Environment and Development (UNCED), promoting criteria and indicators which will help to prevent a further disappearance of some plant species from these modern relics of old vegetation cover and biodiversity (Brand, 1997).

Soil degradation processes in the Savannah region have been linked to population increase and are associated with erosion, soil organic matter loss and decreases in agricultural yields (Poch and Ubalde, 2006; Sebastià et al., 2008). One of the soil degradation processes is the natural or anthropogenic decline in OM (Diwediga et al., 2017; Kintché et al., 2010). This problem is especially severe in tropical soils, with low activity clays and shortage of fertilizers (Lal, 2019; Marks et al., 2009). In the region, forests and woodland have been shown to contain the highest values of soil organic carbon and total nitrogen, whereas agricultural fields exhibited the lowest values (Diwediga et al., 2017) and a positive relationship was found between soil organic matter (OM) and plant

Fig. 2. Study area (Togo West Africa). Left: agricultural field subjected to periodical burning, right: sacred forest remnant.

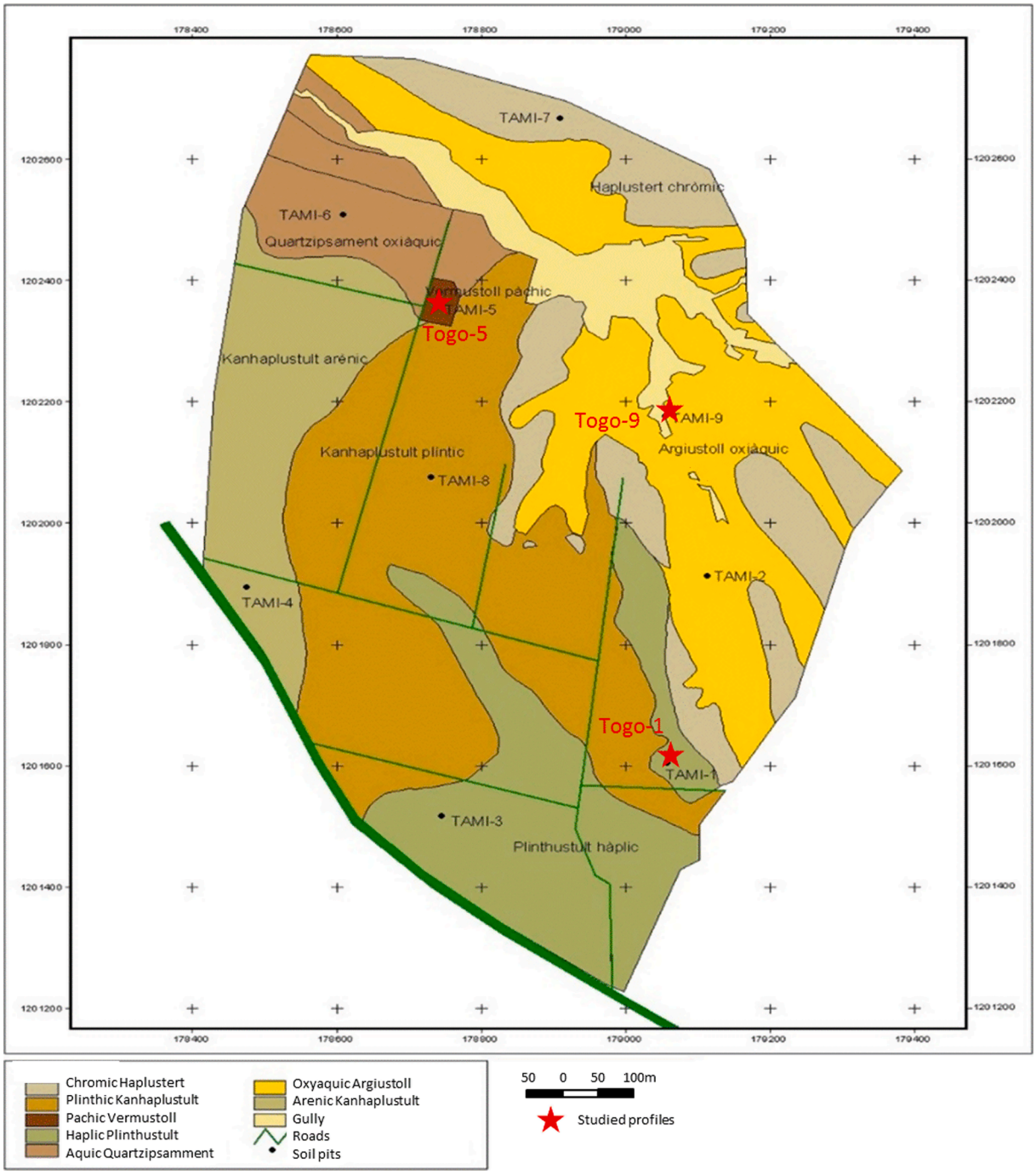

Fig. 3. Soil map of the Tami farm (Poch and Ubalde, 2006) with the location of the three studied profiles (IUSS Working Group, 2015).

biodiversity (Sebastià et al., 2008).

A soil and water conservation project of a farm in Northern Togo having a ¼ ha sacred forest shows very different soil characteristics associated with the soil cover under the forest itself (Ubalde and Poch, 2000). Pedogenic calcite is present in the OM rich soils of the sacred forest, whereas the surrounding soils are very low in organic matter, non-calcareous, moderately acidic, tropical sesquioxide ferruginous soils with ferric concretions and crusts on granites and gneisses (Poch and Ubalde, 2006). These are not pedogenic environments where calcium carbonate accumulations usually occur, as cations are leached, leading to acidification and enrichment of aluminium, silicon, and iron (Pons et al., 2018).

In bio-geology research, it is very important to understand the relationships between organisms and their abiotic environments, which lead to coupled evolution of the biosphere and geosphere. As well as having increased bacterial and fungal populations, the soils with increased organic matter and litter also have increased faunal activity of litter-processors such as oribatid mites, collembola and earthworms, making the biotic contribution to calcium and carbon cycling particularly important in the precipitation of calcium carbonate in organic-rich environments (Castanier et al., 1999; Castro-Alonso et al., 2019; Francis and Poch, 2019; Uren, 2018).

Most of the research on the sacred forests to date has focused on vegetation structure and diversity within the forests (Koutchika et al., 2013) and has not included pedodiversity studies that may explain such variability. In this study, we investigated the morphological,

Table 1
Main morphological characteristics of the selected profiles.

Position & Landuse	Profile and horizons	Depth (cm)	Munsell colour (moist)	Structure (primary, secondary)	Texture (USDA)	Coarse fragments (vol %)	Mottling	Accumulations
Platform	**Profile −1**							
Cotton, corn, peanuts	Ap	0–20	7.5YR4/4	vw-sab-c	LS	16–35	–	–
	Bt1	20–33	10YR6/3	–	SL	>70	–	Silt cutans
	Bts2	33–55	7.5YR5/6	–	SCL	>70	–	Silt cutans, soft concretions
	Bts3	55->60	10R4/6	–	SCL	>70	–	Silt cutans, soft iron matrix
Valley bottom	**Profile −5**							
Sacred forest	Oa	−5- −3	–	–	–	–	–	–
	Oi	−3–0	7.5YR1.7/1	–	–	–	–	–
	A1	0–16/19	7.5YR2/1	vw-c-m, w-sab-m	SC	–	–	–
	Bw1	16/19–43	10YR3/2	w-sab-c	SC	–	–	–
	Bw2	43–75/85	10YR2/3	m-sab-m	SC	–	–	–
	Bwg3	75/85->90	10YR4/3	s-sab-m	SC	1–5	ab-red	Pressure faces
Valley bottom	**Profile −9**							
Pasture rice	Apg	0–20	10YR3/3	w-sab-m	S	5–15	fr-ox	–
	Bg1	20–28	10YR4/6	vw-sab-m	S	5–15	fr-ox	–
	Bst2	28–60	10YR6/6	vw-sab-f	LS	5–15	–	Few clay cutans, Fe-Mn nodules
	Bsm3	60–73	10YR5/6	–	–	16–35	–	Weak Fe cementation
	Bssg4	73–150	2.5YR6/6	vs-sab-f, m-p-c	C	1–5	fr-ox	Abundant slickensides
	C	>150	2.5Y7/2	–	–	–	–	Few silt cutans

Structure: s: strong, m: moderate, w: weak; sab: subangular blocky, g: granular, f: fine, m: medium, c: coarse; **abundance**: -: absent, f: few, c: common, fr: frequent, ab: abundant; **texture**: LS: loamy sand, SL: sandy loam, SCL: sandy clay loam, LS: loamy sand, SC: sandy clay C: clay, **mottles**: ox: oxidation, red: reduction.

microscopic, mineralogical and chemical attributes of various soil horizons that occur in soils from a highly pedodiverse area in Northern Togo (West Africa). Understanding these natural processes is fundamental for implementing soil management practices leading to carbon sequestration and improvement of soil quality status in the region, and possibly in other countries with similar climatic, pedological and geological contexts, and land use/land cover histories.

2. Material and methods

2.1. Study area

The study site covers an area of 100 ha (Latitude 10.859609 Longitude 0.060153) belonging to the Centre de Formation Rurale de Tami, located 20 km east from capital Dapaong (Fig. 1).

The climate is Sudano-Guinean, characterized by a dry season from October to April and a rainy season from May to end of September (Ongoma et al., 2014). According to Köppen–Geiger's classification, northern Togo falls the climate Aw, i.e. tropical savannah or tropical wet and dry climate (Beck et al., 2018). From a 19-year data series from the meteorological station of Dapaong (330 m asl), the mean annual precipitation is 1001 mm, with a maximum in August (266 mm) and a minimum in January (0 mm) with a high inter-annual variability ranging from 649 to 1370 mm in the studied series (Poch and Ubalde, 2006). Both wet and dry rainfall extremes are characteristic (Ali, 2018; Batebana et al., 2015). Annual evapotranspiration is higher than annual precipitation (Gadédjisso-Tossou et al., 2018; Koffi and Komla, 2015), with figures for northern Togo ranging from 1839 mm/year (Koffi and Komla, 2015) to 2057 mm/ year (Poch and Ubalde, 2006). The long-term trend is a decreasing precipitation/evapotranspiration ratio and increasing severity of the aridity index in Togo (Koffi and Komla, 2015). During January and February, the Harmattan, a strong dusty wind from the north east, intensifies the dryness of the season (Poch and Ubalde, 2006). The soil moisture regime is Ustic (Poch and Ubalde, 2006).

The geology of the region mainly includes the sedimentary or epi-metamorphic formations from the Voltaian Basin. The study area is found on the Birrimian (Precambrian) basement consisting of granites, granodiorites, syenites and gneisses (Collart et al., 1985). The rock contains abundant, large, slightly oriented plagioclase crystals, quartz and pegmatitic veins.

The savannah region is characterized by a rolling landscape consisting of sequences of platforms, valleys and slopes, which strongly control the spatial distribution of soil forming and soil erosion processes. These units are found in the study area, at altitudes from 250 to 270 m asl. According to Jones et al. (2013) the predominant soils around Dapaong are Petric Plinthosols and Lithic Leptosols (IUSS Working Group, 2015). They correspond to the tropical sesquioxide ferruginous soils with concretions and crusts on granites, of the historical soil map of Togo 1:1000000 by Lamouroux (1960).

The vegetation is mainly influenced by agriculture activities and typically is woody savannah. Many crops including peanuts, corn, rice, millet, soy and cotton cover the land. The rest are pastures, forest or abandoned cropland. The crop yields are low due to low fertility of the soils and a lack of fertilization: 1850 kg ha^{-1} for corn and 1500 kg ha^{-1} for rice (Poch and Ubalde, 2006). The dominant species are *Parkia biglobosa* and *Butyrospermum parkii* as trees and *Acacia sieberiana* as bush. Riparian and ruderal vegetation are also present. A small remnant of dry Sudanian forest vegetation consisting of *Anogeissus leiocarpus, Butyrospermum parkii, Piliostigma reticulatum* and *Ziziphus mauritiaca* as main species have been preserved as sacred forest (Poch and Ubalde, 2006). In 1973 at the inception of the Centre de Formation Rurale de Tami, the secretary to the Chief of the Tami Canton described the site as being a scrubland with large trees, of which only a few examples remained where an object of veneration by the locals was. He also said that the whole site was considered cursed by the locals (Pan, 2008; Villalabeitia, 2012).

Ubalde and Poch (2000) mapped the soils of the farm at a 1:5000 scale (1 observation/10 ha). They defined the geomorphological and vegetation units used to define soil-mapping units shown in Figs. 1 and 3. The soil units on the platforms (under cotton, corn and peanuts) were classified as Haplic Plinthustult; soil units on the slopes (under soja, corn, peanuts, cotton, millet, sorghum and pasture) were classified as

Table 2
Physicochemical characteristics of the profiles. Classification according to SSS-Soil Survey Staff, (1999) and IUSS Working Group WRB (2015).

Profile	Horizons	Depth (cm)	pH H_2O (1:2.5)	OM (%)	Sand 2 mm-50 μm (%)	Silt 2–50 μm (%)	Clay < 2 μm (%)	CEC cmol+/kg	V (%)	Total Fe g/kg	P g/kg	K g/kg	Mg mg/kg	$N\text{-}NO^{3-}$ mg /kg	$CaCO_3$ (%)
Profile-1	Ap	0–20	5.8	0.6	77.8	11.4	10.8	5	36.1	-	8	37	73	9	None
Haplic Plinthustult;	Bt1	20–33	6.3	0.5	54.8	19.3	25.9	6.2	81.6	38.8	-	32	-	-	None
Pisoplinthic Plinthosol	Bts2	33–55	6.2	0.3	41.3	17.6	41.1	11.7	69.1	73.0	-	44	-	-	None
	Bts3	55–>60	6.0	0.2	36.7	18.3	44.0	11.3	73.1	71.0	-	46	-	-	None
Profile-5	Oi	−3–0	7.7	13.1	-	-	-	-	-	-	15	>600	>600	208	Trace
Pachic Vermustoll;	A1	0–16/19	7.9	9.7	36.8	25.3	37.7	39.1	>98	11.7	15	>600	>600	78	Trace
Pachic Phaeozem	Bw1	16/19–43	8.2	1.6	29.6	23.3	36.9	18.3	100	8.8	3	558	-	-	Trace
	Bw2	43–75/85	8.5	1.6	37.0	23.3	39.7	18.9	100	-	2	550	-	-	Trace
	Bwg3	75/85->90	8.6	0.7	38.7	22.2	39.1	17.8	100	–	2	271	–	–	4
Profile-9	Apg	0–20	6.8	0.9	70.9	15.5	13.6	4.7	60.7	8.2	3	18	87	10	None
Oxyaquic Argiustoll;	Bg1	20–28	7.7	0.3	73.1	13.7	13.2	3.3	70.1	9.5	–	<10	85	–	None
Stagnic Phaeozem	Bst2	28–60	7.8	0.3	61.3	11.1	27.6	6.0	65.3	17.6	–	19	166	–	None
	Bsm3	60–73	7.7	0.2	51.7	9.4	38.9	7.8	73.2	31.4	–	28	236	–	None
	Bssg4	73–150	6.5	0.1	27.4	25.4	47.2	3.9	100	36.1	–	69	561	–	None
	C	>150	8.8	0.0	86.2	7.8	6.0	15.0	22.2	3.3	–	23	137	–	None

Plinthic Kanhaplustult (upslope), Arenic Kanhaplustult (foot slope) and Chromic Haplustert, (eroded slope); the soil units on valley bottoms (under rice and pasture) were classified as Aquic Quartzimsamment and Oxyaquic Argiustoll; and in the valley bottom under the sacred forest the soil classified as Pachic Vermustoll (S.S.S-Soil Survey, 1999). The latter is a natural soil under sacred forest, neutral to basic pH, with calcium carbonate (reacts to 11% HCl), in strong contrast to the soils not under the sacred forest, which were non-calcareous. The soils under agricultural use were severely affected by sheet erosion due to the shape of the fields (slopes too long), sandy texture (low structural stability), and agricultural practices (low organic matter input due to frequent burning of pastures and crop residues) (Poch and Ubalde, 2006).

2.2. Methods

Three of the profiles (profile-1, 5 and 9), representative of different topographic positions, soil types and/or vegetation cover, were selected for micromorphological and mineralogical analyses, and classified according to S.S.S-Soil Survey (1999) and IUSS Working Group (2015). Profile 5 (Pachic Vermustoll; Pachic Phaeozem) is located in the sacred forest in an intermediate-footslope position, whereas profiles 1 (Haplic Plinthustult; Pisoplinthic Plinthosol) and 9 (Oxyaquic Argiustoll; Stagnic Phaeozem) are located upslope (flat landform) and downslope respectively, in the surrounding cultivated savannah (Figs. 1 to 3). These profiles are formed on saprolite of syenites and gneiss. Profile 9 displays in addition a sandy colluvium on top. The soils were surveyed and sampled in two campaigns; 1997 (soil survey, profile description and sampling for micromorphological and physicochemical analyses) and 2006 (surface and subsurface samples for soil mineralogy and selected chemical analyses). Previously published data by co-authors for the same study area were used, including soil maps and physicochemical analyses. In addition, a new detailed micromorphological study and mineralogical analyses were performed on selected soil samples. Brief descriptions of methods are given below. A summary of the field description of profiles 1, 5 and 9 is given in Table 1.

2.2.1. Chemical and physicochemical analyses

Chemical and physicochemical analyses of the three soil profiles were performed in this research according to Porta et al. (1986). The analyses included: particle size distribution (pipette method), organic matter (OM) estimated from organic carbon by wet combustion (Walkley-Black method) using the Van Bemmelen conversion factor (1.72) (Collins and Kuehl, 2001), cation exchange capacity (CEC; ammonium-acetate method), pH (H_2O) in a 1:2.5 soil/water suspension, extractable K and Mg (NH_4-Ac, pH 7), total Fe, P (Olsen). Nitrogen was determined using the Kjehldahl method.

2.2.2. Mineralogy

The clay mineralogy of six samples from the three profiles (0–10 and 20–30 cm depth samples from each profile, representing A and different types of genetic B horizons, such as Bt, Bw and Bg, respectively) was determined using a Philips diffractometer, with Cu-Kα radiation generated at 40 kW and 20 mA. Primary minerals were investigated by X-ray diffraction analysis (XRD) of randomly oriented powder mounts prepared from the sieved fine earth fraction (<2 mm). Clay minerals were detected by X-ray diffractometry after oxidation of OM with H_2O_2 and separation of the clay fraction (<2 μm) after centrifugation. Parallel oriented specimens on glass slides were scanned after the following treatments: Mg-saturation, air-dried and after ethylene–glycol (EG) solvation, K-saturation, air-dried and after heating at 335° and 550 °C.

2.2.3. Micromorphology

Ten horizontal thin sections, 5 × 13 cm in size, were made from undisturbed blocks following the methods of Benyarku and Stoops (2005). They were taken from different soil horizons of profiles 1 (Togo 1), profile 5 (Togo 5), and profile 9 (Togo 9). Thin sections (30 μm thick)

were examined with a polarizing optical microscope and studied following the guidelines of Stoops (2003).

Portions of the uncovered polished blocks were stained with Alizarin red following the method of Proia and Brinn (1985). According to the Alizarin red S staining protocol, calcium deposits except calcium oxalate form an orange-red colour at pH 4.2. Calcium oxalate as well as the carbonate and phosphate stain at a pH of 7. We used the difference in colour development between pH 4.2 and pH 7 to indicate possible areas of calcium oxalate enrichment on the polished blocks (Sikka et al., 2008). The impregnated slabs were washed ultrasonically, dried, and one drop of Alizarin red solution at pH 4.2 was added to a selected area on the slide and left for 3 min. The blocks were washed well with distilled water and photographed. The same area was then treated with Alizarin red solution pH 7 under the same conditions. The blocks were photographed before treatment, after pH 4.2 treatment, and after pH 4.2 + pH 7 treatment in order to track the development of the colour.

3. Results

3.1. Physicochemical characteristics

The chemical and physical features of the representative soils are given in Table 2. The soils contain low OM (<1% dry weight) in profile 1 and profile 9 compared to a considerably higher OM content (13%) in the sacred forest profile 5. The high OM and clay contents in profile 5 are consistent with higher CEC, which indicates a high potential fertility and consistent with the higher topsoil N content in the sacred forest (208 mg $N\text{-}NO_3^-$/kg t for profile 5 compared to 9 and 10 mg $N\text{-}NO_3^-$/kg for profile 1 and 9). The sandy soils are moderately acidic due to base leaching, but without reaching pH values<5.5. In the sacred forest, the soils have a pH consistent with the presence of calcium carbonate, which is present in trace amounts in the upper horizons of the sacred forest profile, increasing with depth, in comparison to the calcite-free savannah soils of the surrounding area.

3.2. Clay mineralogy

The primary minerals in the original gneiss substrate in the region are dominated by quartz, K-feldspar, mica and plagioclases in the Haplic Plinthustult (profile 1), Pachic Vermustoll (profile 5) and Oxyaquic Argiustoll (profile 9). Each topsoil shows the same clay mineral assemblage of the corresponding subsoil horizon analysed, with slight differences in peak intensities, except for profile 5 where smectite and palygorskite peaks were not clear in the topsoil sample in comparison to its subsoil (Figs. 4, 5). The clay fractions of all three profiles display intense reflections typical of kaolinite (especially in profile 1) that disappear after heating at 550 °C, and noticeable but smaller peaks related to illite, extremely weak in the surface horizon of profile 5, which persist after any treatment (Figs. 4, 5). In the samples from profiles 1 and 9 and the 20–30 cm deep sample from profile 5 there is often a double peak around 1 nm (namely 1.0 nm and 1.04 nm), which indicates the presence of illite and possible trace amounts of palygorskite. The

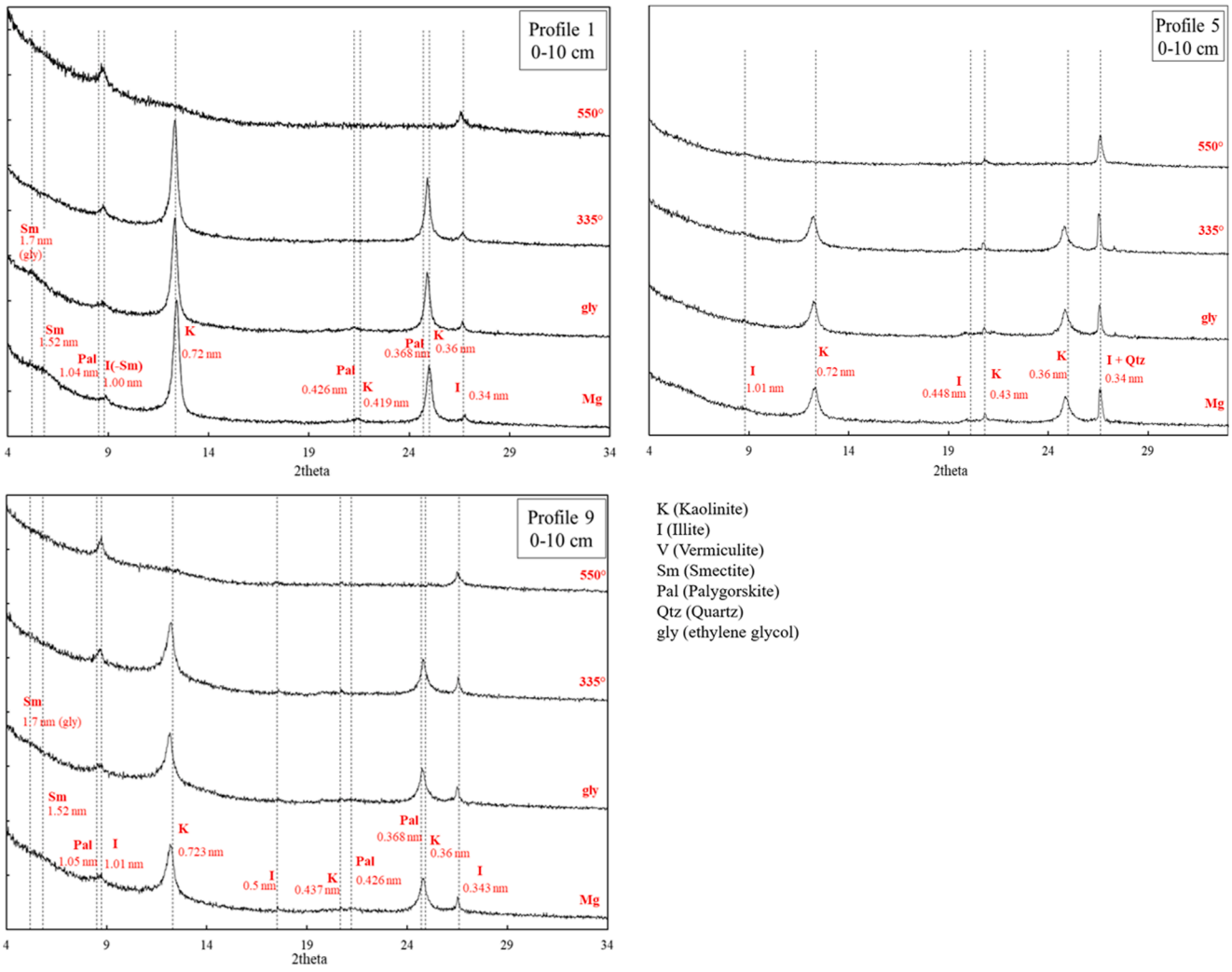

Fig. 4. Mineralogical analysis of clay fraction by XRD (Profile 1, Depth 0–10 cm), (Profile 5, Depth 0–10 cm) and (Profile 9, Depth 0–10 cm).

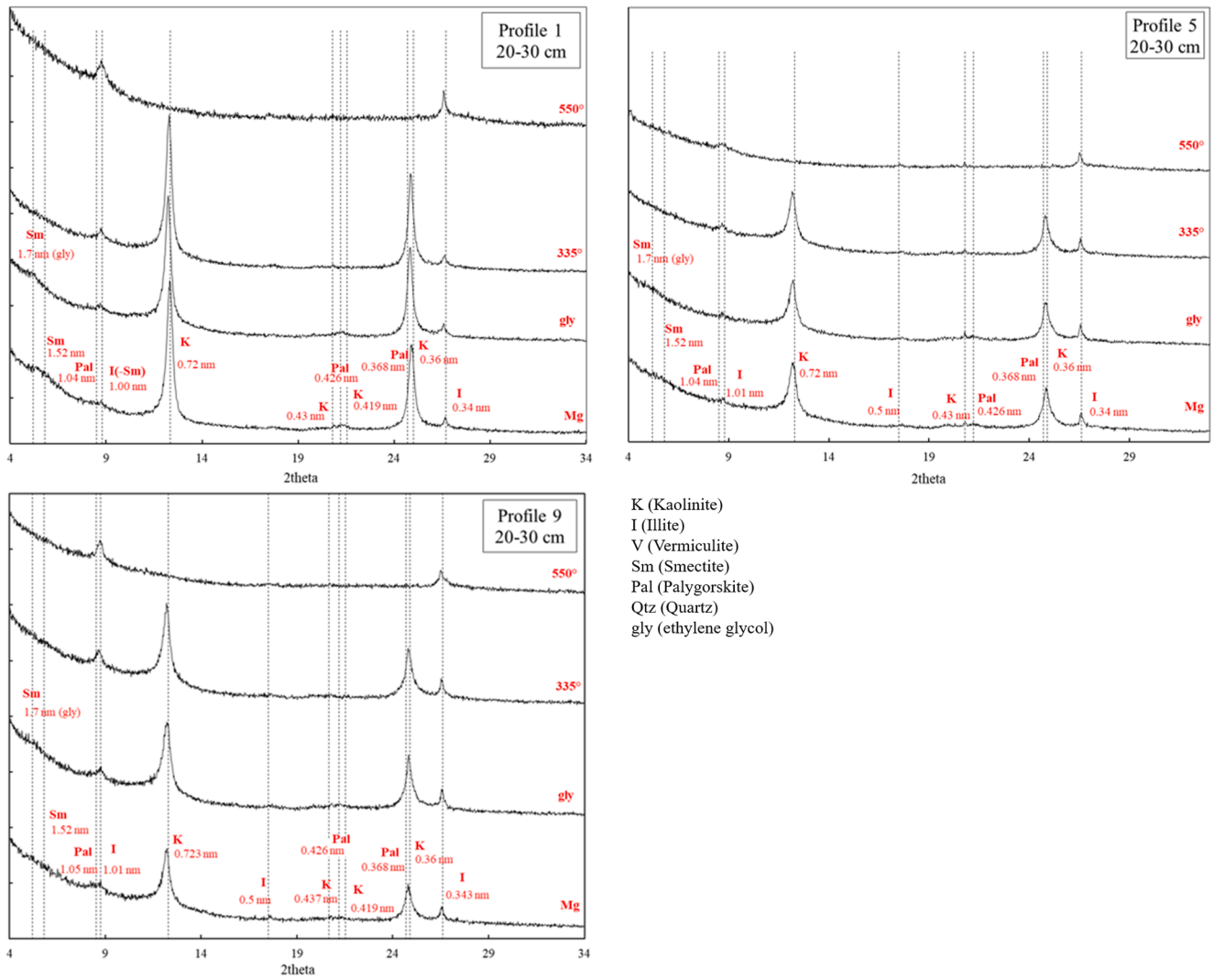

Fig. 5. Mineralogical analysis of clay fraction by XRD (Profile 1, Depth 20–30 cm), (Profile 5, Depth 20–30 cm) and (Profile 9, Depth 20–30 cm).

latter can be supposed by other diagnostic, although weak, reflections at 0.43 and/or 0.41 nm in the three profiles, and a tiny peak/shoulder at 0.365 nm. These peaks disappear on heating, unlike the kaolinite peaks with which they partially overlap (Figs. 4, 5). In profile 1 and 9 and the 20–30 cm deep sample from profile 5, weak peaks of smectite are present, as shown by the 1.5 nm peak expansion to ~ 1.7 nm after ethylene–glycol solvation and collapse to 1.0 nm on heating (Figs. 4, 5). In addition, the illite peak at ca. 1 nm is slightly asymmetrical in all the samples and expands very slightly at its base after glycolation especially in profile 1 (Fig. 4) and possibly in profile 9 (Fig. 4). This behaviour may support the presence of palygorskite and/or of some smectite as mixed layer clay mineral I-Sm. In profile 5, an important diagnostic peak of quartz is also present in the 0–10 cm surface horizon (Fig. 4) that is absent from the 20–30 cm deep horizon (Fig. 5).

3.3. Micromorphology

Despite being very close to each other and developed on the same parent material, the three profiles have very distinct micromorphological characteristics. Some of them are summarized in Table 3.

Profile 1 (Haplic Plinthustult) is characterized by a concentration of Fe oxi-hydroxides as orthic (in situ) and anorthic (transported) nodules. Weathered runiquartz can be observed in profile 1 (Fig. 6a). Clay illuviation can be seen in Fig. 6b. The granostriated b-fabric points to some degree of argilloturbation, which is consistent with the presence of expandable clay minerals in the profile (Fig. 4-profile 1).

The main features of the sacred forest profile 5 (Pachic Vermustoll) are the high OM content and biological activity, shown by the frequent passage features and excrement infillings (Fig. 6c). Other features are Fe-nodules, impregnative Fe-hypocoatings, and different calcitic pedofeatures. The latter consist of:

- prismatic and needle calcite as pore coatings and loose discontinuous infillings, sometimes as stars. They are typically 50–100 μm long and 5–10 μm thick, but they can reach thicknesses up to 50 μm. They are often located around and inside excrements (Fig. 6c, 8d and 9a). These needles were identified as calcite and not as oxalate because they stained with Alizarin red at pH 4.2. (Fig. 7c);
- hypocoatings around pores and nodules made of micrite, also associated with excrements and more frequent in deeper horizons (Fig. 6d and 9c);
- cell pseudomorphs within plant tissues, containing calcium oxalate (Fig. 8a), that stains at pH 7 but not at pH 4.2 (Figs. 7, 8a).

Profile 9 (Oxyaquic Argiustoll) displays different horizon morphologies from the parent material (granite saprolite) to the topsoil compared to the previous profiles (Table 1). The C-horizon is a saprolite composed of quartz, micas and plagioclases altered to illite. The Bg1-horizon shows a slight enrichment of smectite clay (identified in XRD, Fig. 5-profile 9) with respect to the C horizon, and it (Bg1-horizon)

Table 3
Summary of the micromorphology of profiles 1, 5 and 9.

Horizons	Microstructure and Porosity	Micromass and b-fabric	Pedofeatures
Profile 1 (Haplic Plinthustult)			
Bt1 (25–35 cm)	Apedal, total porosity 30%: planar voids, vughs, chambers and channel	Light yellow to brown; silt, clay and organic matter. Granostriated and stipple speckled b-fabric.	Orthic Fe-nodules, very coarse sand size; few silt and clay intercalations; few clay coatings, around fissure walls, limpid, micro-laminated, medium sand size, stained with Fe-oxides; anorthic, concentric Fe-nodules, with inclusions of runiquartz.
Bts2 (30–40 cm)	Weakly developed, separated angular blocky, total porosity 25%, planar voids, channels and chambers	Id previous.	Geodic and concentric Fe-nodules, anorthic, coarse sand size; clay coatings around Fe-nodules; general impregnation of the groundmass with Fe-oxi-hydroxides, with different degrees of intensity.
Bts3 (60–73 cm)	Apedal, vughy, total porosity 20%, vughs and fissures	Id. previous.	Orthic Fe-nodules; frequent clay coatings and infillings, and fragmented clay coatings; anorthic, concentric Fe-nodules, with inclusions of runiquartz.
Profile 5 (Pachic Vermustoll)			
A1 (0–15 cm)	Weakly separated, crumb; total porosity 30%: channels, chambers, fissures, star vughs and compound packing voids.	Yellowish brown and dark brown irregular mixture of amorphous organic matter, fine silt and clay. Stipple speckled b-fabric.	Orthic and rounded anorthic Fe-nodules; few micrite nodules; loose discontinuous infillings of needle calcite; passage features as infilled channels with material from the underlying horizon.
Bw1 (20–30 cm)	Moderately weak subangular blocky, spongy intrapedal microstructure; total porosity 25%: channels and connected chambers, fissures, vughs.	Light yellow to brown, mixture of amorphous organic, fine silt and clay. Stippled speckled, slightly granostriated b-fabric.	Orthic and rounded anorthic Fe-nodules; aggregate Mn nodules; loose discontinuous infillings of needle and prismatic calcite; nodules of micrite associated to faunal excrements.
Bw1 (30–43 cm)	Strong subangular blocky, intrapedal spongy microstructure; total porosity 20%: channels, chambers, vughs, fissures	Yellowish brown, mixture of fine silt, clay and organic matter. Stippled speckled, granostriated b-fabric.	Orthic and rounded anorthic Fe-nodules; aggregate Mn nodules; few 1:1 clay coatings around nodules; loose discontinuous infillings and coatings of needle, prismatic and micritic calcite in pores.
Bwg2 (50–60 cm)	Pedal, weak subangular blocky, intrapedal channel microstructure; total porosity 20%: channels, chambers, fissures, vughs	Yellowish brown, mixture of fine silt, clay and organic matter. Stippled speckled, granostriated b-fabric.	Orthic and rounded anorthic Fe-nodules; aggregate Mn nodules; hypocoatings of micritic calcite; loose discontinuous infillings and coatings of needle and prismatic calcite; rounded nodules of microsparite, medium sand size.
Profile 9 (Oxyaquic Argiustoll)			
Ap (0–13 cm)	Apedal, vughy; total porosity 35%: vughs, channels, chambers, fissures.	Black/brown mixture of fine silt, clay and organic pigments. Undifferentiated b-fabric	Coatings and infillings of mottled clay, microlaminated; frequent impregnative Fe-hypocoatings around channels; orthic and anorthic rounded Fe nodules.
Bst2 (43–60 cm)	Moderately developed subangular blocky; total porosity 30%: channels, chambers, fissures, vughs	Yellow to dark brown mixture of fine silt, clay and organic matter. Granostriated / stipple-speckled b-fabric.	Dusty and limpid clay coatings and intercalations; Fe-nodules, orthic and disorthic; Fe-hypocoatings around channels.
Bssg4 (80–85 cm)	Apedal, spongy microstructure; total porosity 20%: channels, chambers, vesicles, vughs	Yellow to dark brown mixture of fine silt, clay and organic matter. Granostriated / stipple-speckled b-fabric.	Dusty and limpid clay coatings and intercalations; Fe-nodules, orthic and disorthic; Fe-hypocoatings around channels.
Bssg4 (140–155 cm)	Moderately developed subangular blocky microstructure; total porosity 20%: channels, chambers, fissures, vughs.	Greyish yellow mixture of fine silt, clay and organic matter. Grano- and porostriated / stipple-speckled b-fabric.	Microlaminated clay coatings and infillings, some broken and deformed; orthic and disorthic impregnative Fe-nodules and hypocoatings.
C (160–165 cm)	Apedal, single grain; total porosity 10%: very few channels; fissures.	–	Microlaminated clay infillings and coatings in planar voids; neoformed clay (sericite) after plagioclase grains.

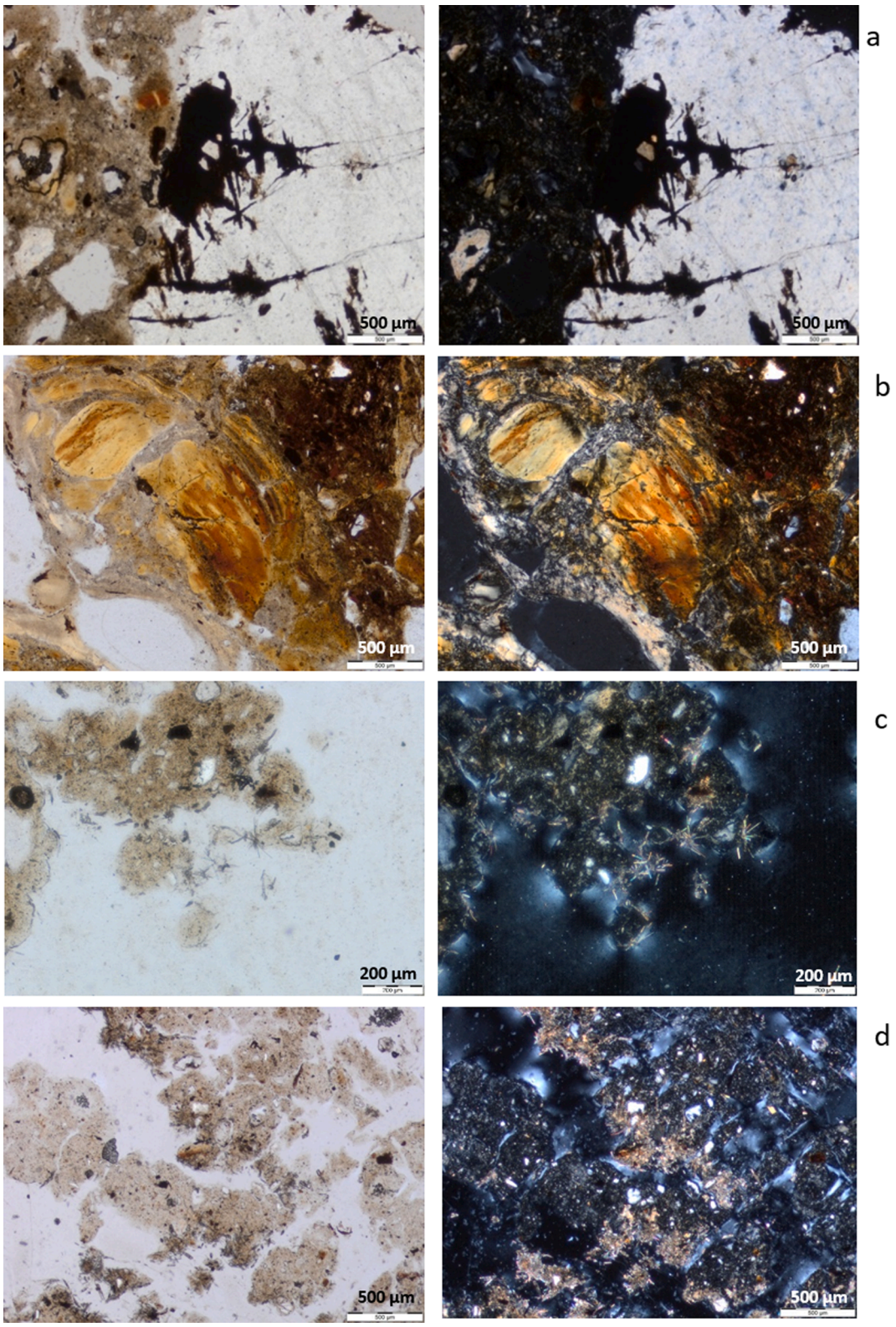

Fig. 6. a: Weathering of quartz and granostriation or stippled speckled and orthic-nodules (Profile 1, 30–40 cm Horizon Bt), b: stress deformed and fragmented clay coatings (Profile 1, 60–73 cm), c: loose infillings of calcite needles in pores near excrements (Profile 5, horizon-Bw), d: impregnative micrite hypocoatings and nodules around excrements (Profile 5, 50–60 cm, horizon Bwg3). Left: plane polarized light (PPL) view; right: crossed polarized light (XPL) view. See Table 3.

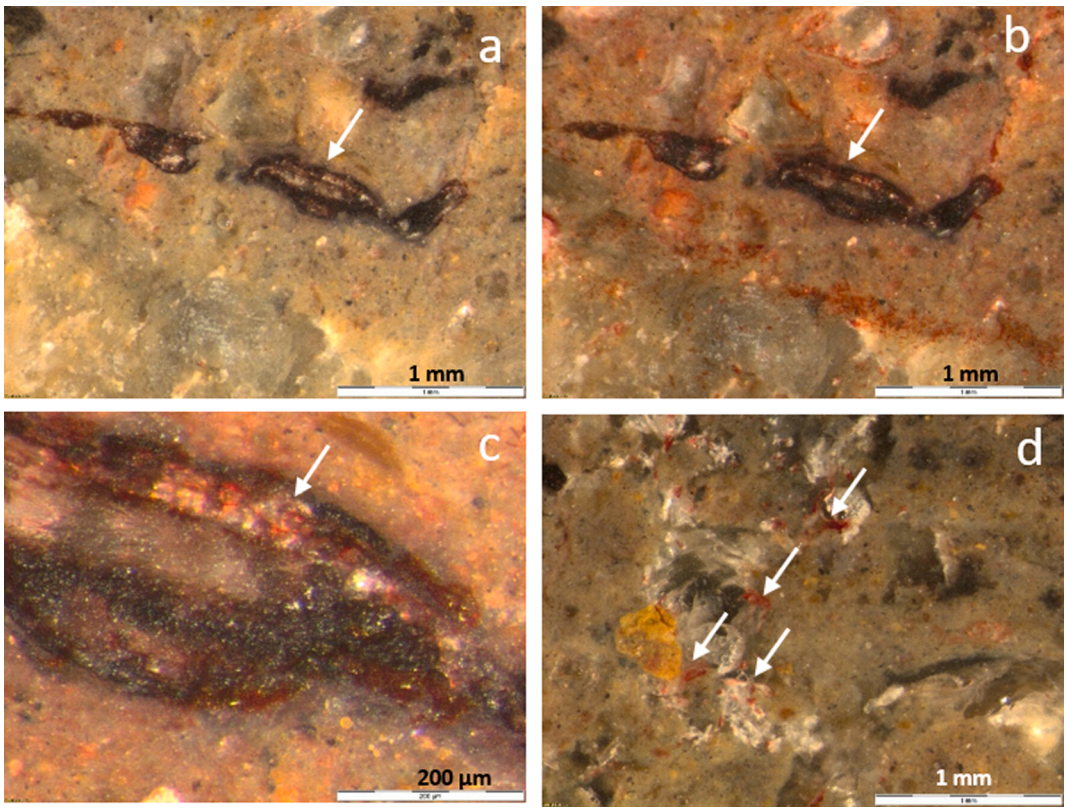

Fig. 7. Binocular images of polished soil faces dyed with Alizarin Red, Profile-5, 50–60 cm. Root section with calcium oxalate crystals, a) after dying at pH 4.2; b) same as a, after dying at pH 7; c) close up of b; d) calcite prisms dyed at pH 4.2 (arrowed). Only the tips of the prisms in contact with the surface are dyed. (For interpretation of the references to colour in this figure legend, the reader is referred to the web version of this article.)

shows both clay illuviation and swelling-shrinking processes (Figs. 6b and 8b). The overlying horizons become more depleted of clay towards the top of the profile and show clear redoximorphic features such as Fe nodules and hypocoatings (Fig. 8b).

4. Discussion

4.1. Clay mineralogy

The clay fractions of all three profiles display intense reflections typical of kaolinite and noticeable peaks related to illite. These clay minerals develop from pedogenesis and chemical weathering processes on primary minerals like feldspars and micas (Scarciglia et al., 2008; Taboada and García, 1999) and are consistent with the basement gneisses and granites as parent materials and with the composition of the Harmatten dust, which seasonally engulfs the study region from its origins in the Chad Basin to the east (He et al., 2007; Lyngsie et al., 2013; Scheuvens et al., 2013). Palygorskite is not typical of the Harmatten dust in the study region (He et al., 2007; Molinaroli, 1996; Moreno et al., 2006; Scheuvens et al., 2013; Singer et al., 2003), suggesting in situ formation. Palygorskite is present in other ustic soil regimes where it is generally inversely correlated with smectite and associated with fluctuating soil moisture conditions (Hashemi et al., 2013; Heidari et al., 2008; Hillier and Pharande, 2008). The presence of trace amounts of palygorskite together with smectite is consistent in this mineralogical context with the extreme wet and dry characteristics of the climate in the region and the current trend toward increasing aridity and intensity of wet-dry extremes (Ali, 2018; Batebana et al., 2015; Koffi and Komla, 2015).

4.2. General pedogenic processes

The studied profiles represent three different situations, having either been formed on saprolites of igneous rocks, on coarse colluvial sands or petroplinthite derived from them.

Profile 1, located on the upper platform (Table 1) is a sandy soil with plinthite, indicated by the presence of weathered quartz, abundant iron oxides, illuvial clays, along with a clay fraction dominated by kaolinite with minor illite. These features indicate that major soil development occurred under prevailing humid and warm climatic conditions, possibly even for long time spans in the past (Agbewornu, 2018; Shanahan et al., 2006). Such environment is/was favourable to intense chemical weathering and leaching processes leading to progressive acidification, possibly coupled with some seasonal contrast promoting removal of clay particles via water suspensions and their down profile migration and stacking within pores, as well as iron release from host minerals and mobility as Fe^{2+} ions, with subsequent reprecipitation in oxy-hydroxides as Fe^{3+} (Scarciglia et al., 2006). Clay illuviation and the granostriated b-fabric point to some degree of argilloturbation, which is in agreement with the presence of smectite in its clay fraction. Given the acidic soil context measured in this soil, the extremely low amount of palygorskite suggests that it could have formed in the past under less acidic soil conditions (initially promoting lesser base leaching such as Mg), which are more suitable for this inverted ribbon aluminosilicate to form. A possible transformation of palygorskite to smectite (Krekeler et al., 2005) could have occurred, confirming that conditions favourable for palygorskite formation were limited to earlier stages of soil formation (Stahr et al., 2000) and that this mineral progressively reduced its amounts to mere traces, in line with the higher degree of development of this profile. Palygorskite is inversely correlated with smectite in similar Ustic soil regimes experiencing strong moisture fluctuations (Hashemi et al., 2013; Heidari et al., 2008; Hillier and Pharande, 2008).

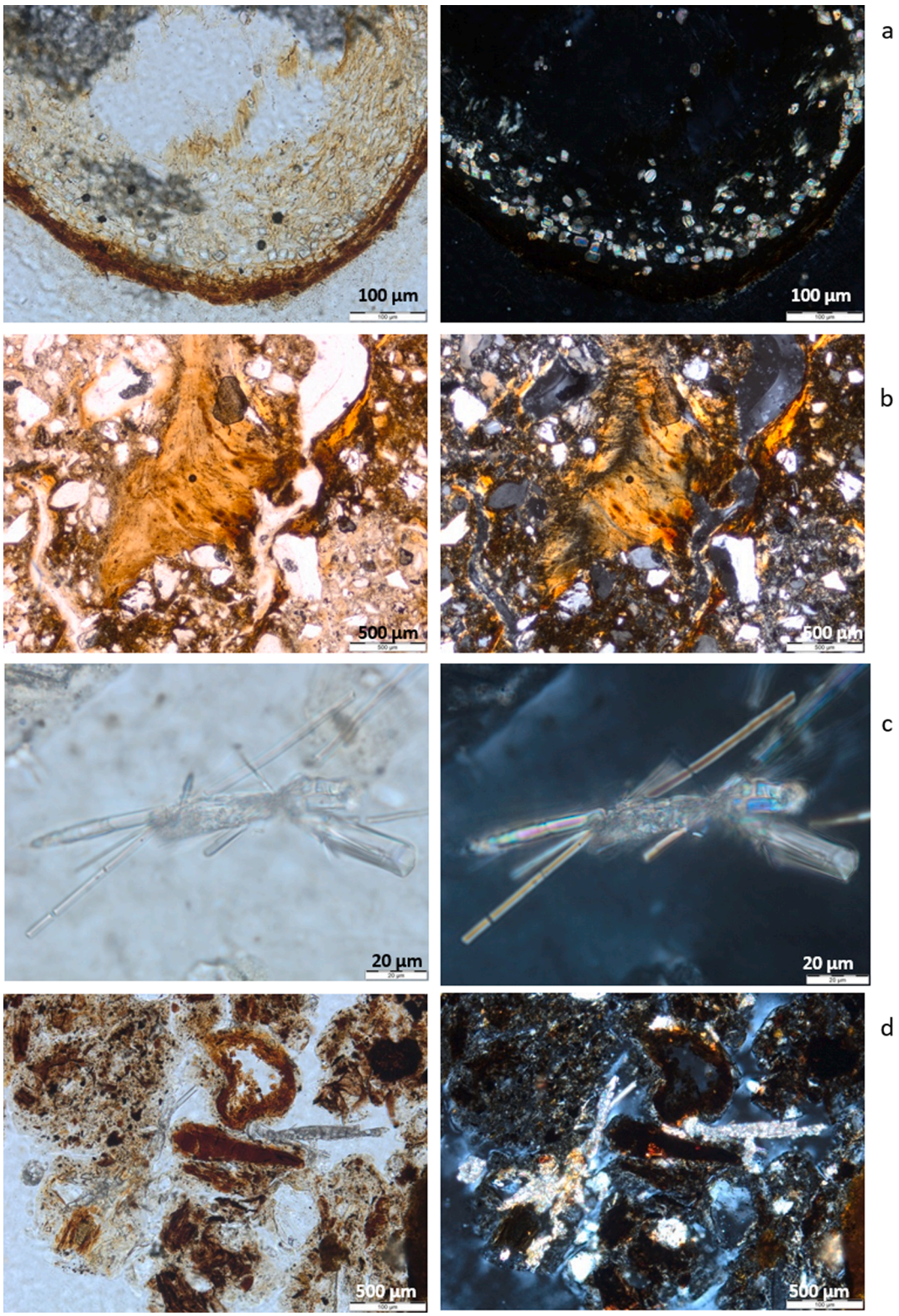

Fig. 8. a: Calcium oxalate crystals inside roots (Profile 5, 0–15 cm Horizon A), b: Reworked clay coating and Fe-oxides hypocoating (Profile 9, 80–85 cm), c: tubes of calcite showing the rounded section and the segmentation in rods, (Profile 5, 50–60 cm) d: polycrystalline needles associated with organic matter. (Profile 5, 0–15 cm). Left: plane polarized light (PPL) view; right: crossed polarized light (XPL) view. See Table 3.

The occurrence of illuvial Bt and Bs horizons at very shallow depths supports that the subsoil could have been truncated by erosion. In addition, the shallow Ap topsoil suggests that erosion still affects the site, likely enhanced by the lack of a protective vegetation cover. Such processes could have led to removal of organic matter and increasing acidification as a result of the human-induced land-use changes (Poch and Ubalde, 2006). The identification of anorthic Fe oxide nodules probably representing fragments of the lower petroplinthite also confirms the anthropogenic disturbance of this profile. All these findings are consistent with the presence of a surface colluvium in profile 9, which

records reworking processes of soil material from upslope.

Profile 5, in the sacred forest, is a Mollisol, and as such its morphology, composition and fertility are very different from the surrounding soils. The main feature is the accumulation of OM, which in the region is related to a high biodiversity (Sebastià et al., 2008), and it may locally be enhanced by rests of animal sacrifices, as the high P content suggests. Harmatten dust is also a source of P and its deposition is enhanced by forest vegetation in the region (Breuning-Madsen et al., 2015). The quartz peak in the clay fraction of the surface of this profile (Fig. 4-profile 5) that is absent from the 20–30 cm depth (Fig. 4b-profile 5) is also consistent with an accumulation of dust-derived fine grained quartz (Scheuvens et al., 2013) at the surface. Both smectite and palygorskite are absent from the surface sample (Fig. 4). The clay mineral assemblage is otherwise similar to that of profiles 1 and 9 for the deeper 20–30 cm horizon (Fig. 4b-profile 9). The main micromorphological features are the different kinds of calcitic features, the weak striation that may be masked by amorphous OM and redoximorphic features such as Fe nodules.

The soil formation processes on the saprolite are fully displayed in profile 9 (Fig. 4-profile 9, and 8b). Profile 9 shows very intense peaks of kaolinite and important peaks of illite (Fig. 4-profile 9). Profile 9 shows frequent slickensides and striated b-fabrics as key feature of swelling clays, as confirmed by XRD data which shows the presence of some swelling smectite (Figs. 4, 5). Part of the clay was later dispersed and illuviated, as evident in the microlaminated clay coatings in these horizons (Fig. 8b). Formation of plinthic horizons would proceed from the more sandy horizons, with Fe-oxide accumulation by direct release from mineral weathering after clay illuviation. The dominance of kaolinite and less developed 2:1 phyllosilicate clays, together with the clay coatings and Fe-oxide features, indicate a high degree of evolution of profile 9 (Fig. 8b), partly similar to profile 1, but probably to a lesser extent, as suggested by smaller kaolinite and higher illite reflections in the XRD patterns. The small amount of smectite is consistent with the evidence of shrink-swell dynamics, as a response to desiccation-imbibition cycles (Scarciglia et al., 2006), identified in thin sections, as well as with partially impeded drainage conditions indicated by the redoximorphic features, hampering removal of basic cations entering such 2:1 phyllosilicate crystal lattice or interlayer. The traces of

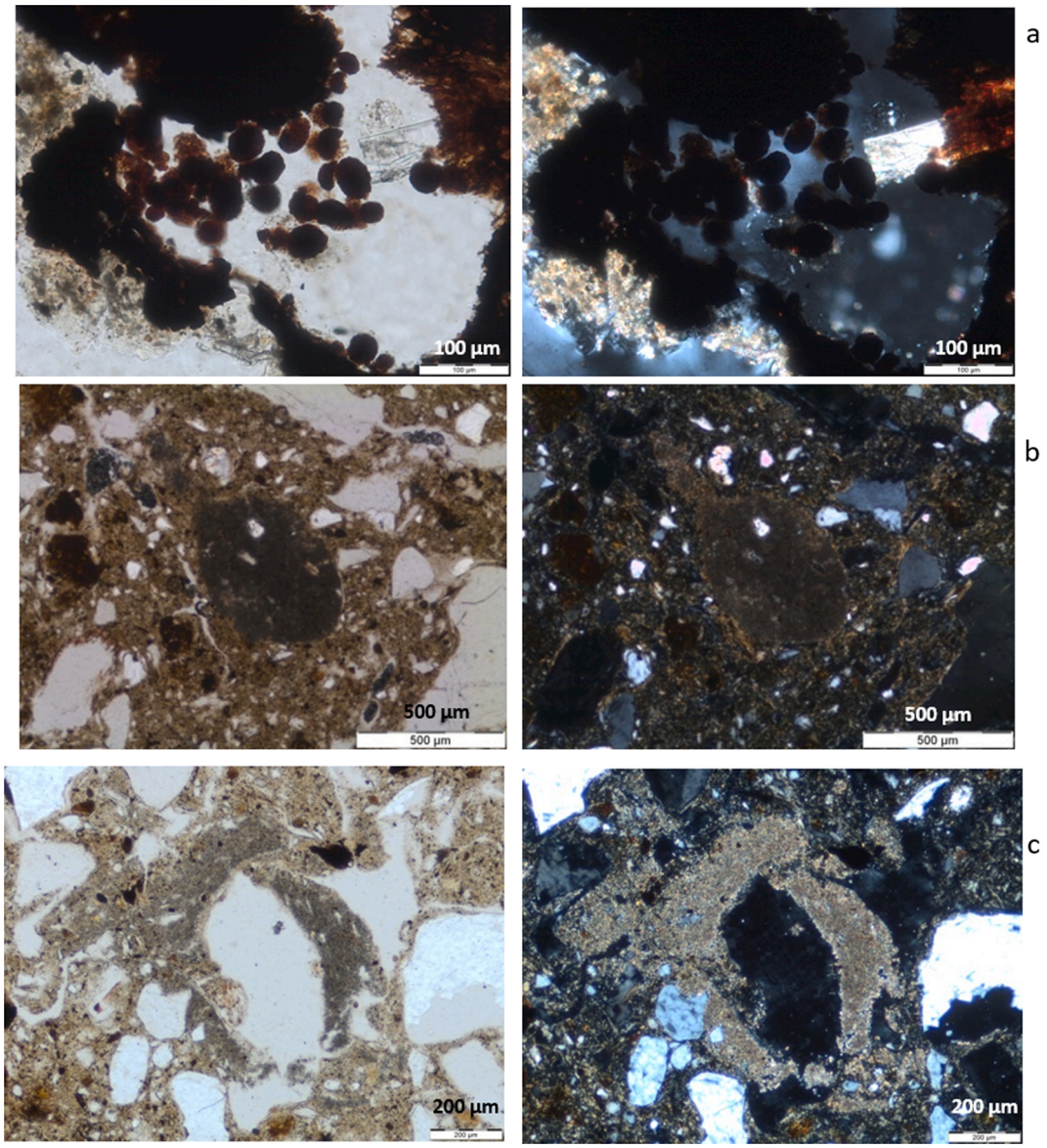

Fig. 9. a: Prismatic calcite crystal next to excrements of Oribatid mites (Profile 5, 20–30 cm), b: Disorthic micrite nodule in a large excrement, note the granostriation around nodules (Profile 5, 50–60 cm), c: Micrite hypocoating (Profile 5, 50–60 cm). Left: plane polarized light (PPL) view; right: crossed polarized light (XPL) view. See Table 3.

palygorskite (Fig. 4-profile 9) may be a relict feature formed under less acidic soil conditions than present, as suggested above for profile 1. However, this clay mineral may also suggest a drastic but likely short shift towards drier soil conditions (Pozo and Calvo, 2018). Further support for fluctuating wet-dry cycles in the profile is the association of small amounts of palygorskite, which is inversely correlated with smectite in similar Ustic soil regimes experiencing strong moisture fluctuations (Hashemi et al., 2013; Heidari et al., 2008; Hillier and Pharande, 2008).

In summary, the main soil formation processes are mineral weathering and 1:1 clay formation, clay illuviation (profile 1 and 9) and redox processes (profile 5 and 9) typical of tropical savannah climates experiencing (all profiles), and OM accumulation and calcite neoformation in profile 5.

4.3. Calcite neoformation in the sacred forest soil

Dietrich et al. (2017) studied the origin of calcium in the secondary carbonate nodules of soils of North Cameroon, developed on granites and greenstones, using the isotope signatures of Sr and Nd. They concluded that the sources of Ca are partly local (weathering of plagioclases and micas) and partly allochthonous (Saharan dust). Since our studied profiles are developed on similar materials and are located in the same climatic belts where they report the occurrence of secondary carbonates (Sudano-Sahelian and Sahelian zones), we could assume the same processes to occur in our soils. However, the fact that calcium carbonate appears throughout the whole profile 5, strongly associated with biological activity only in this profile, and tends to increase in depth (4% at the bottom of the profile), lead us think that allochthonous material is not the main source of calcium or carbonate.

Micromorphology of profile 5 shows the neoformation of calcite as micrite hypo-coatings and nodules, calcified cells and needle calcite in bio-pores, related to biological activity (Fig. 8cd). Some of the neoformed products are most probably not calcite, but calcium oxalate (whewellite) (Fig. 8a). This was the case of the biogenic crystals inside root remains (Fig. 6d and 7a). Prismatic and needle calcite are ubiquitous in calcareous soils (Durand et al., 2010). Needle calcite in its various forms is widely accepted to have biological origin as mounds of fungal sheaths (Bajnóczi and Kovács-Kis, 2006; Cailleau et al., 2009; Milliere et al., 2011; Verrecchia and Verrecchia, 1994). Many crystals of needle calcite, Verrecchia's M and MA types are observed in all horizons of profile 5 (Fig. 9), as coatings or loose discontinuous infillings, often as radial bundles (Fig. 6c and 8b). Sometimes they are composed of a sequence of rods, indicating a biological origin (Fig. 8c). They are normally between 50 and 200 μm long and 3 to 15 μm thick, and their extinction between crossed polarizers is variable. We found also prismatic mono- or polycrystalline calcite with parallel extinction (Fig. 8d and 9d), clearly of inorganic origin (Durán et al., 2010; Jones and Kahle, 1993). Nevertheless, their distribution together with the needle calcite, around plant remains and excrements suggests that biological activity has played a role in their formation. The orthic nodules and hypocoatings of micrite seem also to have the same origin, since they occur together with the previous pedofeatures in microsites with high biological activity such as those with oribatid mite excrements (Fig. 9 abc). Litter transformers such as oribatid mites have been shown to play an important role in calcium recycling and the calcification process in organic matter rich soils (Francis and Poch, 2019). In some cases (Fig. 6c) it is possible to see a transition between calcite needles and micrite, which suggests that at least part of the micrite features comes from a process of dissolution-reprecipitation of the needle calcite, as happens in some petrocalcic horizons (Badía et al., 2009).

The calcium oxalate crystals occur in plant remains (Fig. 6d, 7a and 8a). This is consistent with species of the sacred forest vegetation containing varying amounts of oxalate, from *Butyrospermum Parkii* (0.80% oxalate in the leaves, (Taiwo et al., 2009) and *Anogeissus leiocarpus* (0.58% oxalate in the wood, (Chukwuma and Chigozie, 2016); 0.485 ± 0.22.41% leaves and wood, (Atiku et al., 2016) to *Ziziphus mauritiaca* which has an oxalate content of 15.5% ± 1.50% oxalate in fruit (Umaru et al., 2007) and calcium oxalate in the leaves (Sivasankari and Sankaravadivoo, 2017). Oxalotrophic bacteria and some associated fungi are able to decompose calcium oxalate in vegetation, permitting localized formation of calcium carbonate (Pons et al., 2018, Uren, 2018), which suggests that this process may have contributed to the formation of calcite in the soils associated with high amounts of organic matter. In our case, while oxalic acid is plant produced, calcium was probably present in the soil as a weathering product of the Ca-plagioclases and recycled via biological activity from the calcium-containing plant material. *Butryospermum parkii*, fruits, for example, are a source of calcium (36.4 mg/100 g) while the leaves are also a source of iron (3.80 mg/kg), magnesium (19.16 mg/kg) and potassium (0.61 mg/kg) (Pons et al., 2018; Taiwo et al., 2009).

4.4. The sacred forest soil and inorganic carbon storage

Our data show that the parent material of these soils is not calcareous (Table 2), meaning that these are not lithogenic carbonates and thus making them a carbon sink (Carmi et al., 2019). The presence of needle fiber calcite, not only as fungal biomineralizations (rod-shape) but also as prisms around plant remains and excrements suggests that aerobic biological activity has at least a partial role in the calcite neoformation in the sacred forest soils. This is through the release of CO_2 by respiration, formation of HCO_3^- and precipitation of $CaCO_3$ due to the Ca^{2+} released by the weathering of plagioclases and recycled organic matter (Carmi et al., 2019; Hasinger et al., 2015; Laudicina et al., 2013).

Loss of soil organic carbon is the main driver of soil degradation under human-led disturbance (Diwediga et al., 2017; Kintché et al., 2010). The shape of the sacred forest unit (Fig. 3), with sharp and straight boundaries, strongly suggests that the factors controlling the organic matter accumulation are indeed the vegetation and land use: long term cultivation changed the properties of the soil to such an extent (massive loss of organic matter by mineralisation) that the original state of these soils is no longer evident due to the lack of organic matter (Poch and Ubalde, 2006). Indeed, a very simple estimation of C sequestration shows that while the whole sacred forest profile is storing 227 Mg OC/ha (Sebastià et al., 2008), the amount of stored inorganic carbon considering only 15 cm of the Bwg3 layer with measured 4% of $CaCO_3$ is: 0.15 m * 10,000 m^2/ha * 1,200 kg/m^3 * 0.04 $CaCO_3$ * 0.12C/$CaCO_3$ = 8.64 Mg C/ha. Although this value represents about 4% of the OC, it should be considered as recalcitrant carbon due to the non-leaching character of the Ustic water regime in the region, making preservation of the sacred forest soils essential to both organic and inorganic carbon storage and ecosystem functioning. Our estimation of organic C under sacred forests is not a unique example and evidences are available in the literature of highly varying SOC storage amounts in West African sacred forests, such as 0.65 to 0.90 Mg OC/ha (Falade and Taiwo, 2020); 100 to 120 Mg OC/ha (to 30 cm depth, Oyelowo et al., 2019), 95.1 Mg OC/ha (to 30 cm depth, Anikwe, 2010) or 42.1 Mg OC/ha (to 10 cm depth, Areola et al., 1982). However, no information was provided in these studies related to inorganic C, which we have found in our study. This highlights the need for more work on mechanisms and magnitude of inorganic carbon storage in soils.

5. Conclusions

The results of the analyses show a high degree of weathering of the gneiss parent materials, presence of plinthite gravels, prevalence of 1:1 clays, formation of swelling clays in the imperfectly drained soils, and low organic matter (OM) in the agricultural soils. In the natural, OM rich soils under forest, bio-calcification takes place and litter recycling has played an important role in cation accumulation and the formation of calcite. The soil characteristics found under the Togo forest indicate a high potential for development of the soils of the area in agroforestry,

agricultural yields and in potential carbon sequestration relevant to global change policies.

Declaration of Competing Interest

The authors declare that they have no known competing financial interests or personal relationships that could have appeared to influence the work reported in this paper.

References

Agbewornu, K., 2018. Global warming and water resources variability in the maritime region of Togo (West Africa). Environment and Natural Resources Research 8, 49.

Ali, E., 2018. Impact of climate variability on staple food crops production in Northern Togo. J. Agric. Environ. Int. Dev. 112, 321–342.

Anikwe, M.A., 2010. Carbon storage in soils of Southeastern Nigeria under different management practices. Carbon Balance Manage. 5 (1), 5.

Areola, O., Aweto, A., Gbadegesin, A., 1982. Organic matter and soil fertility restoration in forest and savanna fallows in southwestern Nigeria. GeoJournal 6, 183–192.

Atiku, A., Oladipo, O., Forcados, G., Forcados, Mancha, M., 2016. Anti-nutritional and phytochemical profile of some plants grazed upon by ruminants in North Central Nigeria during the dry season (January to April). International Journal of Livestock Production 7, 19–23.

Badía, D., Martí, C., Palacio, E., Sancho, C., Poch, R.M., 2009. Soil evolution over the Quaternary period in a semiarid climate (Segre river terraces, northeast Spain). CATENA 77, 165–174.

Bajnóczi, B., Kovács-Kis, V., 2006. Origin of pedogenic needle-fiber calcite revealed by micromorphology and stable isotope composition—a case study of a Quaternary paleosol from Hungary. Geochemistry 66, 203–212.

Batebana, K., et al., 2015. Rainfall characteristics over Togo and their related atmospheric circulation anomalies. Journal of Environmental and Agricultural Sciences 5, 34–48.

Beck, H.E., et al., 2018. Present and future Köppen-Geiger climate classification maps at 1-km resolution. Sci. Data 5, 1–12.

Benyarku, C.A., Stoops, G., 2005. Guidelines for preparation of rock and soil thin sections and polished sections. Quaderns DMACS, 33, Universitat de Lleida, Lleida.

Bhaghwat, S.A., Kushalappa, C.G., Williams, P.H., Brown, N.D., 2005. Landscape approach to biodivesity in Western Ghats of India. Conserv. Biol. 19, 1853–1862.

Brand, D.G., 1997. Criteria and indicators for the conservation and sustainable management of forests: Progress to date and future directions. Biomass Bioenergy 13, 247–253.

Breuning-Madsen, H., Awadzi, T.W., Lyngsie, G., 2015. Deposition of nutrients from Harmattan dust in Ghana, West Africa. Pedosphere 25, 613–621.

Cailleau, G., Verrecchia, E.P., Braissant, O., Emmanuel, L., 2009. The biogenic origin of needle fibre calcite. Sedimentology 56, 1858–1875.

Campbell, M.O., 2004. Traditional forest protection and woodlots in the coastal savannah of Ghana. Environ. Conserv. 31, 225–232.

Carmi, I., Kronfeld, J., Moinester, M., 2019. Sequestration of atmospheric carbon dioxide as inorganic carbon in the unsaturated zone under semi-arid forests. Catena 173, 93–98.

Castanier, S., Le Métayer-Levrel, G., Perthuisot, J.P., 1999. Ca-carbonates precipitation and limestone genesis — the microbiogeologist point of view. Sed. Geol. 126, 9–23.

Castro-Alonso, M.J., et al., 2019. Microbially induced calcium carbonate precipitation (MICP) and its potential in bioconcrete: microbiological and molecular concepts. Front. Mater. 6, 126.

Ceperley, N., Montagnini, F., Natta, A., 2010. Significance of sacred sites for riparian forest conservation in Central Benin. Bois et Forêts des Tropiques 303.

Chukwuma, S.E., Chigozie, M.E., 2016. Qualitative and quantitative determination of phytochemical contents of indigenous Nigerian softwoods. New Journal of Science 2016, 9.

Collart, J., Ouassane, I., Sylvain, J.P., 1985. Notice explicative de la carte géologique à 1/200 000. Feuille Dapaong, 1e Édition". Mémoire. 2. République Togolaise, Ministère de l'Equipment, des Mines et des Postes et Télécommunications, DG Mines. Géologie et du Bureau National des Recherches Minières.

Collins, M.E., Kuehl, R.J., 2001. Organic matter accumulation and organic soils. In: Richardson, J.L., Vepraskas, M.J. (Eds.), Wetland soils. Genesis, hydrology, landscapes, and classification. Lewis, CRC, Boca Raton, pp. 137–162.

Daye, D.D., Healey, J.R., 2015. Impacts of land-use change on sacred forests at the landscape scale. Global Ecol. Conserv. 3, 349–358.

Dietrich, F., et al., 2017. Origin of calcium in pedogenic carbonate nodules from silicate watersheds in the Far North Region of Cameroon: respective contribution of in situ weathering source and dust input. Chem. Geol. 460, 54–69.

Diwediga, B., Le, Q.B., Agodzo, S., Wala, K., 2017. Potential storages and drivers of soil organic carbon and total nitrogen across river basin landscape: The case of Mo river basin (Togo) in West Africa. Ecol. Eng. 99, 298–309.

Durán, J., Rodríguez, A., Fernández-Palacios, J.M., Gallardo, A., 2010. Long-term decrease of organic and inorganic nitrogen concentrations due to pine forest wildfire. Annals of Forest Science 67, 207.

Durand, N., Monger, H.C., Canti, M.G., 2010. Chapter 9 - Calcium carbonate features. In: Stoops, G., Marcelino, V., Mees, F. (Eds.), interpretation of micromorphological features of soils and regoliths. Elsevier, Amsterdam, pp. 149–194.

Fairhead, J., Leach, M., 1998. Reconsidering the extent of deforestation in twentieth century West Africa. Unasylva 49, 38–46.

Falade, O.F., Taiwo, A.J., 2020. Forest structure and carbon stocks of Osun-Osogbo Sacred Grove, Nigeria. International Journal of Biodiversity and Conservation 12, 25–32.

Francis, M.L., Poch, R.M., 2019. Calcite accumulation in a South African heuweltjie: Role of the termite Microhodotermes viator and oribatid mites. J. Arid Environ. 170, 103981.

Fraser, J.A., et al., 2016. Cultural valuation and biodiversity conservation in the Upper Guinea forest, West Africa. Ecol. Soc. 21.

Gadédjisso-Tossou, A., Avellán, T., Schütze, N., 2018. Potential of deficit and supplemental Iirrigation under climate variability in Northern Togo. West Africa. Water 10, 1803.

Hashemi, S., Baghernejad, M., Najafi, G.M., 2013. Clay Mineralogy of Gypsiferous Soils under Different Soil Moisture Regimes in Fars Province. Iran. Journal of Agricultural Science and Technology 15, 1053–1068.

Hasinger, O., et al., 2015. Carbon dioxide in scree slope deposits: A pathway from atmosphere to pedogenic carbonate. Geoderma 247, 129–139.

He, C., Breuning-Madsen, H., Awadzi, T.W., 2007. Mineralogy of dust deposited during the Harmattan season in Ghana. Geografisk Tidsskrift-Danish Journal of Geography 107, 9–15.

Heidari, A., Mahmoudi, S.H., Rouzi, T.M.H., Mermut, A., 2008. Diversity of clay minerals in the Vertisols of three different climatic regions in Western Iran.

Hillier, S., Pharande, A., 2008. Contemporary pedogenic formation of palygorskite in irrigation-induced, saline-sodic, shrink-swell soils of Maharashtra, India. Clays Clay Miner. 56, 531–548.

Irakiza, R., et al., 2016. Assessment of traditional ecological knowledge and beliefs in the utilisation of important plant species: The case of Buhanga sacred forest. Rwanda. Koedoe 58 (1), 1–11.

IUSS Working Group, W., 2015. World Reference Base for Soil Resources 2014, update 2015 International soil classification system for naming soils and creating legends for soil maps. World Soil Resources Reports No. 106. FAO, Rome.

Jones, A., et al., 2013. Soil Atlas of Africa. European commission, publications office of the European Union, Luxembourg, p. 176 pp..

Jones, B., Kahle, C.F., 1993. Morphology, relationship, and origin of fiber and dendrite calcite crystals. J. Sediment. Res. 63 (6), 1018–1031.

Kibet, S., 2011. Plant communities, species diversity, richness, and regeneration of a traditionally managed coastal forest, Kenya. For. Ecol. Manage. 261, 949–957.

Kintché, K., Guibert, H., Sogbedji, J., Levêque, J., Tittonell, P., 2010. Carbon losses and primary productivity decline in savannah soils under cotton-cereal rotations in semiarid Togo. Plant Soil 336, 469–484.

Koffi, D., Komla, G., 2015. Trend analysis in reference evapotranspiration and aridity index in the context of climate change in Togo. J. Water Clim. Change 6, 848–864.

Kokou, K., Adjossou, K., Kokutse, A.D., 2008. Considering sacred and riverside forests in criteria and indicators of forest management in low wood producing countries: The case of Togo. Ecol. Ind. 8, 158–169.

Kokou, K., Dzifa, A., 2007. Conservation de la biodiversité dans les forêts sacrées littorales du Togo: Diversité biologique. Bois et forêts des tropiques 292, 59–70.

Kokou, K., Sokpon, N., 2006. Les forêts sacrées du couloir du Dahomey. Bois et Forêts des Tropiques 2 (288), 15–23.

Koutchika, R.I., Agbani, P.O., Sinsin, B., 2013. Influence des perturbations anthropiques sur la biodiversité des bois sacrés du Centre Bénin. International Journal of Biological and Chemical Sciences 7, 306–318.

Krekeler, M.P.S., Hammerly, E., Rakovan, J., Guggenheim, S., 2005. Microscopy Studies of the Palygorskite-to-Smectite Transformation. Clays Clay Miner. 53 (1), 92–99.

Lal, R., 2019. Tropical soils: distribution, properties and management. Tropical Resources: Ecology and Development 3, 39–52.

Lamouroux, M., 1960. Notice Explicative No 34. Carte Pédologique du Togo au 1/1,000,000. Service Cartographique de l'ORSTOM, Centre ORSTOM Lomé.

Laudicina, V.A., Scalenghe, R., Pisciotta, A., Parello, F., Dazzi, C., 2013. Pedogenic carbonates and carbon pools in gypsiferous soils of a semiarid Mediterranean environment in south Italy. Geoderma 192, 31–38.

Lyngsie, G., Olsen, J.L., Awadzi, T.W., Fensholt, R., Breuning-Madsen, H., 2013. Influence of the inter tropical discontinuity on Harmattan dust deposition in Ghana. Geochem. Geophys. Geosyst. 14 (9), 3425–3435.

Marks, E., et al., 2009. Conservation of soil organic carbon, biodiversity and the provision of other ecosystem services along climatic gradients in West Africa. Biogeosciences 6 (8), 1825–1838.

Milliere, L., et al., 2011. Stable carbon and oxygen isotope signatures of pedogenic needle fibre calcite. Geoderma 161, 74–87.

Molinaroli, E., 1996. Mineralogical characterisation of Saharan dust with a view to its final destination in Mediterranean sediments, The impact of desert dust across the Mediterranean. Springer 153–162.

Moreno, T., et al., 2006. Geochemical variations in aeolian mineral particles from the Sahara-Sahel Dust Corridor. Chemosphere 65, 261–270.

Ongoma, V., et al., 2014. Rainfall characteristics over Togo and their related atmospheric circulation anomalies. J. Environ. Agric. Sci. 5, 34–48.

Oyelowo, O., Aduradola, A., Sulaiman, O., Aina-oduntan, O., 2019. Physico-chemical characteristics of soil in two sacred graoves of Western Nigeria. Ethiopian Journal of Environmental Studies & Management 12 (4).

Pan, S., 2008. Histoire de Tami. PROYDE. https://www.proyde.org/libros/Histoire_Tami.pdf.

Poch, R.M., Ubalde, J.M., 2006. Diagnostic of degradation processes of soils from northern Togo(West Africa) as a tool for soil and water management. Workshop IC-PLR.

Pons, S., et al., 2018. Biocontrolled soil nutrient distribution under the influence of an oxalogenic-oxalotrophic ecosystem. Plant Soil 425 (1), 145–160.

Porta, J., López-Acevedo, M., Rodríguez, R., 1986. Técnicas y experimentos en edafología. Col· legi Oficial d'Enginyers Agrònoms de Catalunya, Barcelona, Spain.
Pozo, M., Calvo, J.P., 2018. An overview of authigenic magnesian clays. Minerals 8 (11), 520.
Proia, A., Brinn, N., 1985. Identification of calcium oxalate crystals using alizarin red S stain. Arch. Pathol. Lab. Med. 109 (2).
S.S.S-Soil Survey, S., 1999. A basic system of classification for making and interpreting soil surveys. USDA, Washington.
Sanou, L., Devineau, J.L., Fournier, A., 2013. Groupements floristiques et capacité de régénération des espèces ligneuses des sanctuaires boisés dans l'aire culturelle bwaba (département de Bondoukuy, Ouest Burkinabé). Acta Botanica Gallica 1, 77–102.
Scarciglia, F., Pulice, I., Robustelli, G., Vecchio, G., 2006. Soil chronosequences on Quaternary marine terraces along the northwestern coast of Calabria (Southern Italy). Quat. Int. 156, 133–155.
Scarciglia, F., Rosa, R., Vecchio, G., Apollaro, C., Robustelli, G., 2008. Volcanic soil formation in Calabria (southern Italy): The Cecita Lake geosol in the late Quaternary geomorphological evolution of the Sila uplands. J. Volcanol. Geoth. Res. 177 (1), 101–117.
Scheuvens, D., Schütz, L., Kandler, K., Ebert, M., Weinbruch, S., 2013. Bulk composition of northern African dust and its source sediments—A compilation. Earth Sci. Rev. 116, 170–194.
Sebastià, M.T., Marks, E., Poch, R.M., 2008. Soil carbon and plant diversity distribution at the farm level in the savannah region of Northern Togo (West Africa). Biogeosciences 5, 4107–4127.
Shanahan, T., et al., 2006. Paleoclimatic variations in West Africa from a record of late Pleistocene and Holocene lake level stands of Lake Bosumtwi, Ghana. Palaeogeogr. Palaeoclimatol. Palaeoecol. 242, 287–302.
Sikka, S., Selwitz, C., Doehne, E., Chiari, G., Khanjian, H., 2008. Qualitative and Quantitative Methods of Detection and Mapping of "Calcium Oxalate Deposits" on Treated Limestones and Marbles, Stone Consolidation in Cultural Heritage: Research and Practice; Proceedings of the International Symposium, Lisbon, 6–7 May 2008, pp. 445-454.
Singer, A., Ganor, E., Dultz, S., Fischer, W., 2003. Dust deposition over the Dead Sea. J. Arid Environ. 53, 41–59.
Sivasankari, M.P., Sankaravadivoo, A., 2017. Leaf anatomical studies of ziziphus mauritiana lam. Biosciences and plant biology 4, 73–79.
Stahr, K., et al., 2000. Palygorskite-cemented crusts (palycretes) in Southern Portugal. Soil Res. 38, 169–188.
Stoops, G., 2003. Guidelines for analysis and description of soil and regolith thin sections. Soil Science Society of America, Madison, WI.
Taboada, T., García, C., 1999. Pseudomorphic transformation of plagioclases during the weathering of granitic rocks in Galicia (NW Spain). Catena 35, 291–302.
Taiwo, A., Oyedepo, J., Oluwadare, I.M.O., 2009. Nutrient content and anti-nutritional factors in shea butter (Butryospermum parkii) leaves. Afr. J. Biotechnol. 8, 5888–5890.
Ubalde, J.M., Poch, R.M., 2000. Projet de conservation des sols et des eaux dans la zone soudano-guinéenne au Centre de Formation Rurale de Tami (Togo). Bulletin du Réseau Erosion 20, 485–495.
Umaru, A., Adamu, R., Dahiru, D., Margret, N., 2007. Levels of antinutritional factors in some wild edible fruits of Northern Nigeria. Afr. J. Biotechnol. 6.
Upadhaya, K., Pandey, H.N., Law, P.S., Tripathi, R.S., 2003. Tree diversity in sacred groves of the Jaintia hills in Meghalaya, northeast India. Biodivers. Conserv. 12, 583–597.
Uren, N.C., 2018. Calcium oxalate in soils, its origins and fate – a review. Soil Res. 56, 443–450.
Verrecchia, E.P., Verrecchia, K.E., 1994. Needle-fiber calcite; a critical review and a proposed classification. J. Sediment. Res. 64, 650–664.
Villalabeitia, J., 2012. Sembrando futuro. PROYDE, www.proyde.org/libros/Sembrando_Futuro_Josean_Villalabeitia.pdf.